Journal of Power Sources 207 (2012) 91–100

Contents lists available at SciVerse ScienceDirect

Journal of Power Sources

journal homepage: www.elsevier.com/locate/jpowsour

Effect of microporous layer on MacMullin number of carbon paper gas diffusion layer

Michael J. Martínez-Rodríguez[a,1], Tong Cui[a], Sirivatch Shimpalee[a,*], Supapan Seraphin[b], Binh Duong[b], J.W. Van Zee[a]

[a] Department of Chemical Engineering, University of South Carolina, Columbia, SC 29208, USA
[b] Department of Materials Science and Engineering, University of Arizona, Tucson, AZ 85721, USA

ARTICLE INFO

Article history:
Received 15 November 2011
Received in revised form 19 January 2012
Accepted 21 January 2012
Available online 9 February 2012

Keywords:
MacMullin number
Effective diffusion
Pore size distribution
Gas diffusion layer
Fuel cells

ABSTRACT

The effect of the microporous layer (MPL) and wet proofing on the MacMullin number has been evaluated for a custom series of Toray TGP-H-060 carbon paper gas diffusion layer (GDL). Complementary characterizations for these GDLs were performed by using scanning electron microscopy (SEM) images, pore size distribution (PSD) and fuel cell performance. The GDLs were customized by the addition of a microporous layer (MPL) and the treatment of, either or both, the substrate and MPL with 10% and 40% hydrophobic agent. SEM images correlated very well with the data shown for PSD. Distinction between the substrate layer and the MPL were clearly shown as two different slopes in the integral distribution and two different peaks in the differential distribution. The MacMullin number increased with increase in wet proofing but decreased with the addition of the MPL. The MacMullin number is a key parameter that contains the missing information for the path length in GDLs, which is generally approximated with the Bruggeman expression. The results provided an overview for the interpretation of the combined effect of the substrate and MPL properties as well as the cell operating conditions.

1. Introduction

Development of low-cost gas diffusion layers (GDL) with tailored properties is a key factor in the optimization of fuel cell performance. The functionality of the GDL inside the fuel cell relies in maintaining a balance between its mechanical, electrical, thermal and transport properties. A GDL must be able to provide mechanical support to the membrane electrode assembly (MEA), conduct electrons between the catalyst layer (CL) and bipolar plates, allow heat removal and maintain uniform temperature, and transport reactant gases to the CL and liquid water away from the CL. As fuel cells become attractive as power sources for automotive, stationary and portable applications a large amount of effort has been dedicated on research to understand and improve GDL properties [1].

Research has demonstrated that the addition of a thin layer to the surface of the GDL results in a positive effect in the performance of the fuel cell [2–4]. Therefore, most GDLs for commercial polymer electrolyte membrane fuel cell (PEMFC) generally consist of a dual-layer carbon-based porous media as shown in Fig. 1. The layer adjacent to the flow field channels is a carbon substrate macroporous layer. The carbon substrate can be either a carbon cloth or a carbon paper and can be impregnated with a hydrophobic agent, such as polytetrafluoroethylene (PTFE). The layer adjacent to the catalyst layer consists of a thinner microporous layer (MPL) typically made of carbon black powder with a hydrophobic agent as well. The purpose of the microporous layer is to minimize the contact resistance between the macroporous layer and the catalyst layer, limit the loss of catalyst to the GDL interior and help to prevent water accumulation within the pore volume of the microporous layer thus gases can freely contact the catalyst sites.

Due to the importance of the MPL into balancing the transport of reactant gases and the removal of liquid water many recent studies have focused on investigating the properties of the MPL. Accordingly, attention has been given to the effect of MPL arrangement in terms of including the MPL in the cathode alone, in both anode and cathode, and without MPL [5], including a double MPL [6], preparation method [7,8], composition [9,10], pore structure [11,12], thickness [13], and wettability, by looking at either hydrophobic [14,15] or hydrophilic [16,17] components. Experimental measurements have been performed for GDLs with MPL that include through – plane permeability [18], pressure vs saturation curves [19], and dynamic drainage [20]. Also, significant modeling efforts have been devoted to understanding the interaction of the key

* Corresponding author. Tel.: +1 803 576 6140; fax: +1 803 777 8265.
E-mail address: shimpale@cec.sc.edu (S. Shimpalee).
[1] Present address: Savannah River National Laboratory, Aiken, South Carolina 29808, USA.

0378-7753/$ – see front matter © 2012 Elsevier B.V. All rights reserved.
doi:10.1016/j.jpowsour.2012.01.132

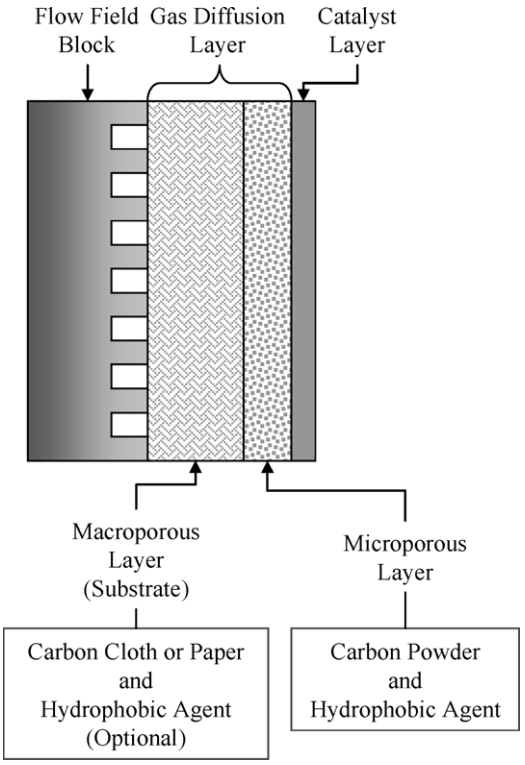

Fig. 1. Schematic of dual-layer carbon-based GDL (not to scale).

parameters of the MPL that affect fuel cell performance [21–30]. The reported results have provided valuable insight to the function of the MPL. However, more research is still required to reach a complete understanding of the individual and combined characteristics of the MPL.

An experimental study has been performed to characterize carbon cloth and carbon paper GDLs in terms of the MacMullin number [31] which relates the bulk properties with the effective transport in the porous media as

$$N_M = \frac{D}{D_{\text{eff}}} = \frac{\sigma}{\sigma_{\text{eff}}} \tag{1}$$

where D and D_{eff} are the bulk and effective diffusion coefficients of the gas in the GDL and; σ and σ_{eff} are the bulk and effective ionic conductivity of the liquid in the GDL saturated with an electrolyte, respectively. The MacMullin number is a parameter determined only by the morphology of the GDL and can be expressed as a generalized relationship with tortuosity (τ) and porosity (ε):

$$N_M = f(\tau, \varepsilon) = \frac{\tau^n}{\varepsilon^m} \tag{2}$$

where n and m are constants that depend on the geometrical model used to describe the porous media [32] or can be determined empirically.

Under some conditions of an operating fuel cell, pores in the GDL can be filled with liquid water, which effectively decreases the porosity for the gas stream. To account for this effect, an effective porosity is generally used

$$\varepsilon_{\text{eff}} = (1 - s)\varepsilon \tag{3}$$

where s represent the average liquid saturation in the GDL. Consequently, Eq. (2) can be expressed in terms of an effective MacMullin number as

$$N_{M,\text{eff}} = f(\tau, \varepsilon, s) = \frac{\tau^n}{(1 - s)^m \varepsilon^m} \tag{4}$$

Note that factors such as GDL compression and wet proofing treatments also affect the morphology of the GDL or the MacMullin number due to changes in the porosity and tortuosity.

Similar studies have been performed for some carbon paper GDLs. Baker et al. [33,34] used limiting current measurements to estimate the oxygen transport resistance in the GDL at different pressures. From these measurements values of D/D_{eff} (or MacMullin number) were computed for the GDLs as function of GDL thickness and compression. These values were found to have relatively good agreement with *ex situ* measurements of D/D_{eff} for water vapor diffusion through the same material. Although they also used GDLs with MPL, their results showed no significant change in the transport resistance as compared to the GDLs without MPL to which it was attributed that the MPL has nearly the same effective diffusion as the substrate. However, this conclusion is imprecise as discussed by the authors. Caulk and Baker [35] used GDLs with MPL but their measurements of D/D_{eff} were performed for the substrate only. Kramer et al. [36] and Flückiger et al. [37] used the analogy of diffusion and ionic conduction described in Eq. (1) and applied electrochemical impedance spectroscopy to measure the ratio of $\sigma_{\text{eff}}/\sigma$ (or inverse of MacMullin number) for different carbon paper GDLs. In this study the effect of direction (in-plane and through-plane), compression, binder structure and hydrophobic treatment were investigated. However, the GDLs used for obtaining the measurements do not have MPL.

The effect of the MPL on the MacMullin number is still unclear. In this study a custom series of Toray TGP-H-060 was selected for characterization and extend on previous work [31]. This series consist of carbon paper GDLs with and without MPL and with different amount of wet proofing treatment. This work will help to assess the effect of the GDL structure, particularly the MPL, in the MacMullin number. However, in order to understand the GDL structure changes with respect to the MacMullin number measurements, scanning electron microscopy (SEM) images and pore size distribution (PSD) were also performed. Finally, the MacMullin number N_M was correlated with the results of the fuel cell performance.

2. Experimental

2.1. Materials

Toray TGP-H-060 was selected as the base GDL for this work. This is a carbon paper GDL which includes only the substrate layer with no wet proofing treatment and has a nominal thickness of 190 μm. Additional GDLs were customized by BASF Fuel Cell, Inc. with the addition of a MPL and the treatment of, either or both, the substrate and MPL with 10% and 40% hydrophobic agent. The amount of wet proofing was selected for research purposes. In order to accurately measure the MacMullin number several GDLs need to be stacked and a significant difference in the wet proofing will also help to evaluate its effect accordingly. Table 1 details the layers and wet proofing for the custom series of these GDLs.

2.2. Characterization techniques

The techniques used to characterize the Toray custom series consist of scanning electron microscopy (SEM) images, pore size distribution (PSD), the MacMullin number N_M, and polarization curves. A 1 cm × 1 cm strip of each sample was cut with clean scissors and mounted onto a SEM flat stub with an adhesive tape for plan view imaging. For cross-section imaging, the sample was mounted on a 90° angle stub. All the SEM images were taken using a Hitachi field-emission SEM S-4800 at an operating voltage of 15 kV. The pore distribution was assessed by using mercury intrusion porosimetry with a Micromeritics Autopore IV mercury

Table 1
Toray custom series used for characterization.

GDL	Layers and wet proofing				Overall porosity[a]	SEM		
	Substrate	Wet proofing	MPL	Wet proofing		X-Section (Fig. 2)	Substrate Side (Fig. 3)	MPL Side (Fig. 4)
1	√	0%	–	–	0.80	(a)	(a) and (b)	–
2	√	10%	–	–	0.78	(b) and (d)	(c)	–
3	√	10%	√	10%	0.75	(e)	–	(e)
4	√	10%	√	40%	0.74	(f)	–	(f)
5	√	40%	–	–	0.69	(c) and (g)	(d)	–
6	√	40%	√	10%	0.68	(h)	–	(g)
7	√	40%	√	40%	0.69	(i)	–	(a)–(d) and (h)

[a] Values obtained from Hg intrusion porosimetry.

porosimeter. The effect of pressure, PSD technique, and the type of GDL in the PSD measurements are discussed in Martinez et al. [38]. The MacMullin number was measured as described in details by Martinez et al. [31]. Finally, polarization curves were used to determine the effect of the GDL on fuel cell performance.

2.3. Fuel cell setup and polarization measurements

A fuel cell hardware from Fuel Cell Technologies, Inc. with an active area of 25 cm^2 was employed in the tests. The cell consisted of triple serpentine flow field plates with anode and cathode co-current flows. In the experiments PRIMEA® 5631 MEAs from W.L. Gore & Associates, Inc. were used. The MEAs consisted of 0.45 mg Pt–Ru cm^{-2} in the anode, 0.6 mg Pt cm^{-2} in the cathode, and a membrane with 35 μm nominal thickness. Toray custom series was employed as GDL as described above. Silicone coated glass fiber (SCF1007), with a thickness of 178 μm, from Saint Gobain was used as gasket during the assembly of the cell. The cell was compressed with a torque of 113 N cm per bolt.

The experiments were conducted using a fuel cell test station model 890B from Scribner and Associates Inc. High purity hydrogen (99.999%) and compressed air were supplied to the anode and cathode respectively. All experiments were performed at 70 °C with pressures of 101 kPa on the anode and the cathode. The flow rates were set to maintain a fixed stoichiometry of 1.2 with a minimum flow of 84 sccm for the anode and 2.0 with a minimum flow of 332 sccm for the cathode. Each cell tested was broken-in in three steps by setting the temperatures of the cell/anode/cathode to 50/50/40 °C, 60/65/55 °C and 70/80/70 °C for 24 h at each step while the cell was maintained at a constant potential of 0.6 V. Cell polarizations using each GDL from the Toray custom series were performed at two humidity conditions corresponding to anode/cathode temperatures of 65/55 °C (designated as low humidity) and 85/75 °C (designated as high humidity). The voltage-current curves were obtained by changing the cell voltage from open circuit to 0.2 V. At each point the voltage was maintained for 15 min and the average of the current during the last minute was recorded.

3. Results and discussion

The effect of the treatment on the structure of the GDL was examined using high-resolution SEM. The microstructure of the Toray custom series in cross-sectional view are shown in Fig. 2 while plane view of the substrate surface and the microporous layer (MPL) are shown in Figs. 3 and 4, respectively. See Table 1 for details on the corresponding conditions of sample treatments.

Fig. 2 shows cross-sectional view of the microstructure of the GDLs. Fig. 2a clearly show the fibers that constitute the bare substrate with no wet proofing. However, comparing Fig. 2d 10% wet proofing of the substrate and Fig. 2g 40% wet proofing of the substrate with Fig. 2a the bare substrate, we can observe materials that filled in between fibers. Nevertheless, there are no noticeable differences between the two wet proofing treatments that have been applied to the substrate. Fig. 2e, f, h and i shows the GDL after adding the MPL. The images reveal a merge between the substrate and the MPL instead of a well defined and a clear boundary. Also, Fig. 2 shows that the treatment in the substrate or MPL did not affect considerably the thickness of these layers. The thickness range of the substrate was estimated between 190 and 200 μm while the MPL was estimated to be between 90 and 100 μm. The thickness of the MPL represents 1/3 of the total thickness, which is 2× the thickness used by Baker et al. [34]. However, their results did not show an effect due to the MPL. Conversely, thicker MPLs have been used in studies of MPL design parameters on permeability and fuel cell performance [39,40]. The thicker MPL was intended to magnify the effect on the measurements of the MacMullin number.

Fig. 3a and b show the microstructure of the substrate composed of carbon fiber having an average diameter of 8.1 μm. Differences in the substrate layer due to the surface treatment are shown in Fig. 3c and d. A considerable reduction in open space (porosity) can be observed between the GDL substrate (Fig. 3a) and the GDL with 10% wet proofing (Fig. 3c). The GDL with 40% wet proofing (Fig. 3d) shows more web-like material between the fibers as compared to the GDL with 10% wet proofing. SEM images of other samples with MPL before and after the wet proofing (not shown here) reveal no significant differences in the microstructure of the substrate side of the GDL.

The MPL structure is shown in Fig. 4. Cracks on the surface of the MPL side of sample 7 (GDL with 40% wet proofing in the MPL) can be observed in Fig. 4a and at higher magnifications from 200× in Fig. 4b to 5000× in Fig. 4d. The width of the cracks is ranging between 4.4 μm to 32 μm. These cracks were also observed in all of the GDLs that have MPL. Additional low vacuum SEM images were taken to verify if the vacuum used during the regular SEM images could have developed cracks in the MPL. The low vacuum SEM images (not shown) indicate that the cracks are in the samples and were not caused by the vacuum of the SEM instrument. These cracks could have developed due to handling of the GDL or perhaps during the drying process when the MPL is added to the GDL. Cracks in the MPL act as mesopores or macropores which affect the MPL porosity [41] and have a significant role in the liquid and gas transport through this layer [23,42]. The microstructure of the MPLs with 10% wet proofing is shown in Fig. 4e and g while that of the MPLs with 40% wet proofing is shown in Fig. 4f and h. The distribution of pore size is 0.02 μm to 0.75 μm as shown on the images for selected pores. There are no observable structural differences of the MPL due to the treatments in the substrate and the MPL.

The effect of the wet proofing and the MPL in the PSD are shown in Figs. 5–7. Fig. 5a and b compare the PSD of Toray carbon paper GDL without the MPL. These curves are characterized by a steep slope around a pore size of 30 μm. This region is shown as one main peak in the differential distribution (Fig. 5b), which represent the substrate region or macroporous layer. The curves show a volume

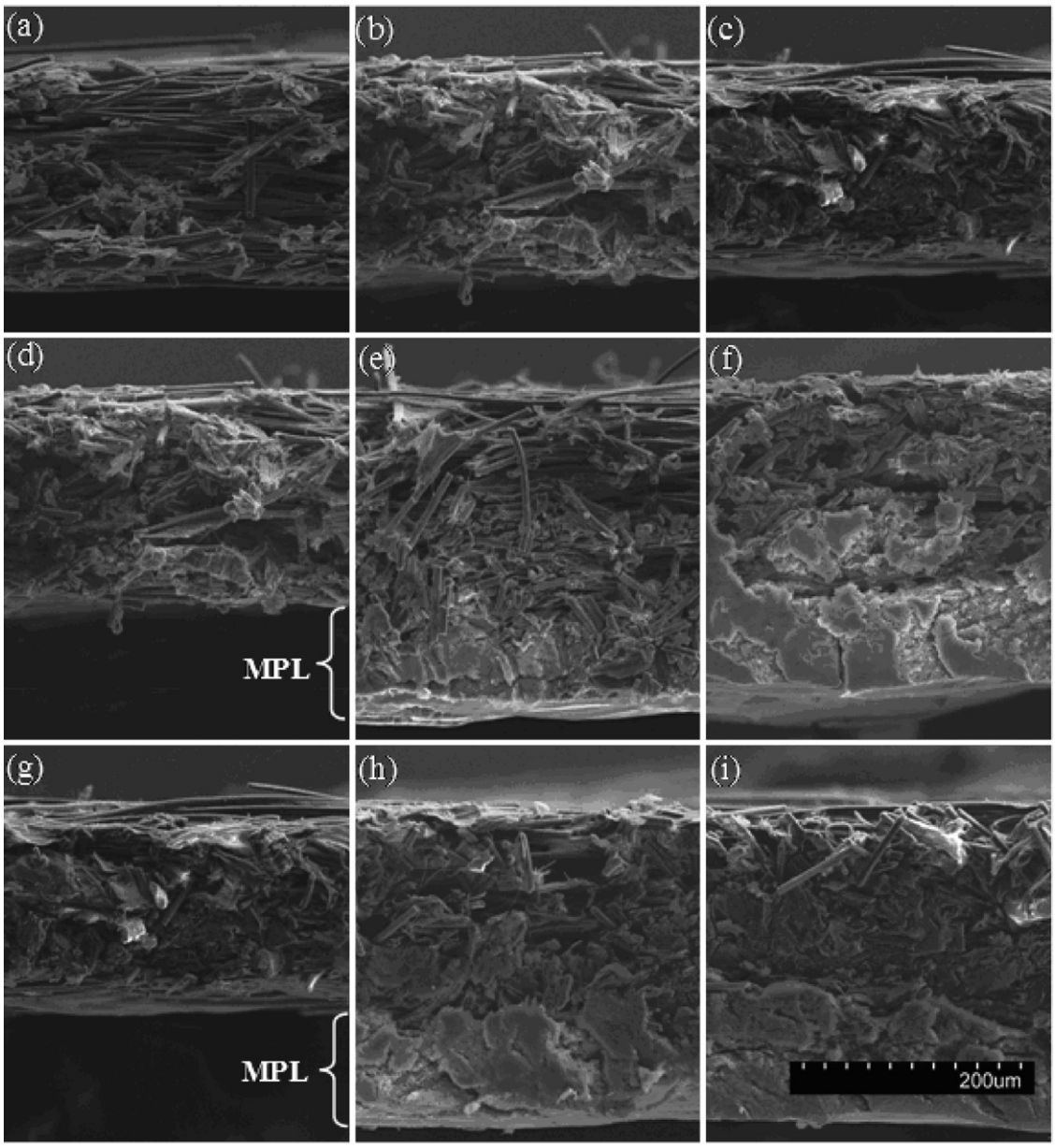

Fig. 2. Scanning electron microscope (SEM) images showing cross-sections of Toray TGP-H-060. (a) The GDL substrate; (b) and (d) the GDL with 10% wet proofing in the substrate; (c) and (g) the GDL with 40% wet proofing in the substrate; (e) the GDL with 10% wet proofing in the substrate and 10% in the MPL; (f) the GDL with 10% wet proofing in the substrate and 40% in the MPL; (h) the GDL with 40% wet proofing in the substrate and 10% in the MPL; (i) the GDL with 40% wet proofing in the substrate and 40% in the MPL.

reduction in the GDLs as the wet proofing increases. This reduction in volume correlates with the reduction in open space observed in Fig. 2 and is in agreement with literature for overall porosity decrease with increase of wet proofing [43–45]. Fig. 6a and b compare the PSD of Toray carbon paper GDL with and without the MPL when the wet proofing in the substrate is 10%. The curves for the GDLs with MPL are characterized by two slopes around 0.05 μm and 30 μm. The slope around 0.05 μm corresponds to the MPL and it appears as one main peak in the differential distribution (Fig. 6b). However, when the MPL is present the volume in the substrate region is reduced. The reduction in volume in the substrate can be explained by the merging of the MPL with the substrate as shown in Fig. 2. Penetration of the MPL into the substrate has been reported in the literature [41,46]. In addition, there is no considerable change in volume for the MPL due to the wet proofing. Fig. 7a and b compare Toray carbon paper GDL with and without the MPL when the wet proofing in the substrate is 40%. These GDLs show the same characteristics as the GDLs with 10% wet proofing in terms of microporous and macroporous distribution and the volume reduction in the substrate when the MPL is present.

Fig. 8 shows the results for the MacMullin number studies in this work. Fig. 8a presents the effect of the total thickness of GDLs stacked on the MacMullin number. Toray carbon paper without wet proofing and MPL (GDL 1) was used for this test. The thickness of this GDL is approximately 200 μm. The value of the MacMullin number decreased as the total thickness of the GDLs stacked increased until it reaches a stable value at the total thickness of 600 μm. Therefore, in this work the number of paper GDLs required to produce consistent data were 4–5 pieces. The MacMullin number obtained for the GDL 1 was 3 which has relative good agreement with values reported in the literature. Baker et al. [33,34] reported ~2.8 (as read from the figure) for the uncompressed and untreated Toray TGP-H-060 from *ex situ* measurements of D/D_{eff} in a diffusion cell. Using in situ measurements of limiting current they calculated

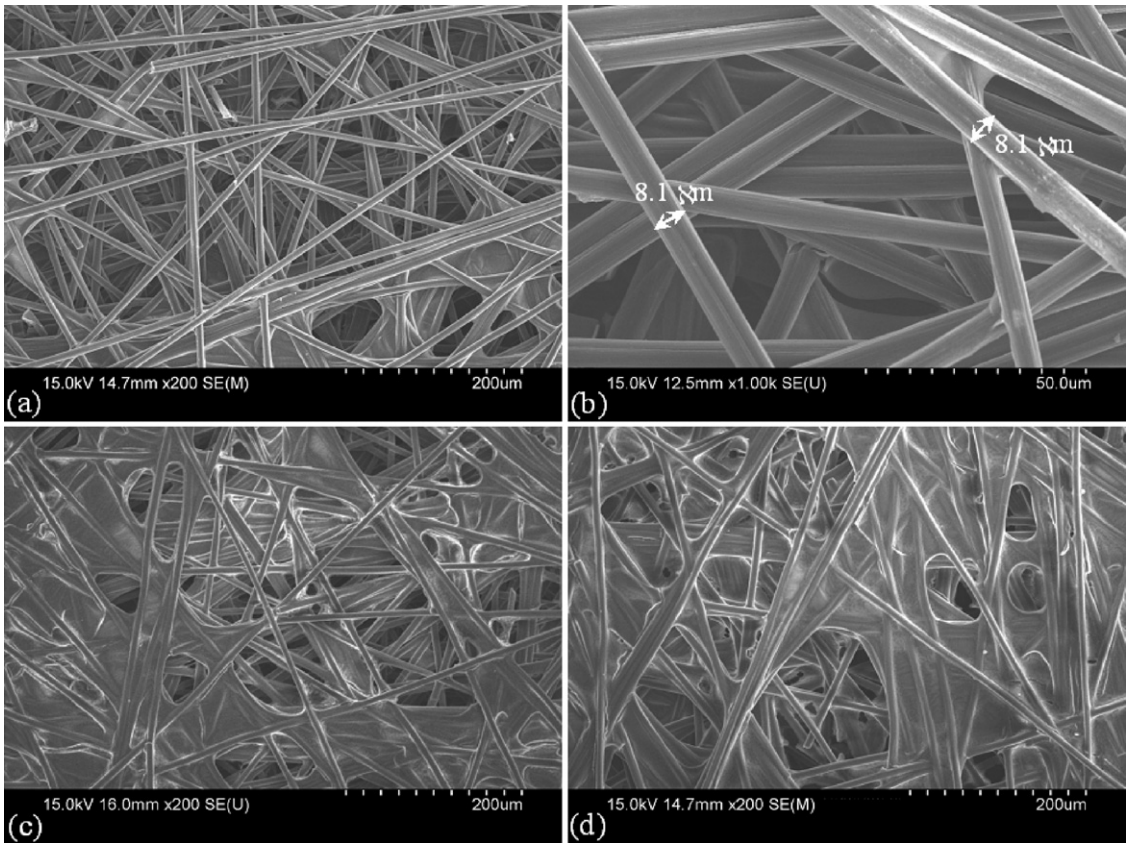

Fig. 3. Scanning electron microscope (SEM) images showing the substrate side of Toray TGP-H-060. (a) and (b) the GDL substrate; (c) the GDL with 10% wet proofing in the substrate; (d) the GDL with 10% wet proofing in the substrate.

an average value of 3.20 [34]. Flückiger et al. [37] reported $\varepsilon/\tau \approx 0.35$ (as read from the figure) for the same GDL, which corresponds to a MacMullin number of 2.86. The effect of the wet proofing and the MPL on the MacMullin number is shown in Fig. 8b. It can be observed that the addition of wet proofing increases the MacMullin number. Increasing the wet proofing will decrease the porosity of the substrate layer as described above and will increase the tortuosity as well. Consequently, a higher flow resistance is expected as porosity decreases and tortuosity increases as described in Eq. (2). However, the addition of the MPL decreases the MacMullin number. This effect could be related to the different wet proofing treatments of the substrate and the MPL, which can cause an additional driving force in the liquid through the pores during the experiments, and perhaps an effect that is magnified due to the small pores in the MPL. Even when the treated surfaces have the same wet proofing percentage the actual contact angle in each surface could be

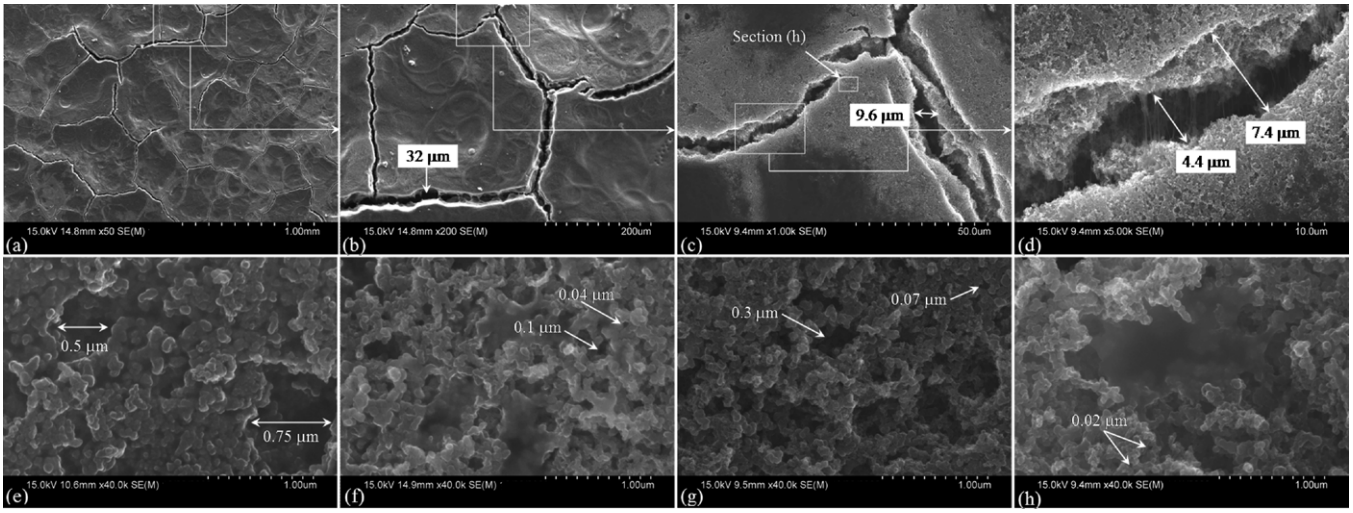

Fig. 4. Scanning electron microscope (SEM) images showing the MPL side of Toray TGP-H-060. (a)–(d) A sequence of images at higher magnifications of the GDL with 40% wet proofing in the substrate and 40% in the MPL showing numerous surface cracks; (e) the GDL with 10% wet proofing in the substrate and 10% in the MPL; (f) the GDL with 10% wet proofing in the substrate and 40% in the MPL; (g) the GDL with 40% wet proofing in the substrate and 10% in the MPL; (h) the GDL with 40% wet proofing in the substrate and 40% in the MPL.

Table 2
Changes in GDL properties and effect in cell performance.

Toray TGP-H-060	Structure change	Wet proofing		ε	N_M [a]	κ [50–53] [b]	κN_M	Cell performance[c]	
		Substrate	MPL					@ RHL	@ RHH
Substrate only	Increasing wet proofing in substrate	↑	–	↓	↑	?	?	↷	↓
Sub10 & (Sub10 + MPL)	Adding MPL to Sub10	10%	–	↓	↓	↓	↓	↓	↓
Sub40 & (Sub40 + MPL)	Adding MPL to Sub40	40%	–	No Δ	↓	↓	↓	↑	↑
Sub10 + MPL	Increasing wet proofing in MPL of Sub10	10%	↑	No Δ	No Δ	↓	↓	↑	↑
Sub40 + MPL	Increasing wet proofing in MPL of Sub40	40%	↑	No Δ	No Δ	↓	↓	No Δ	Slightly ↓

Sub10, Sub40, substrate with 10% and 40% wet proofing, respectively. No Δ, no change or about the same value. ?, Cannot be determined with the given information.
[a] The effect of the MPL could be related more to the liquid transport as compared to the gas transport for which an effective N_M can be calculated from Eq. (4).
[b] The effect of κ was interpreted based on the results of the given references.
[c] Cell performance for humidity conditions designated as low (RH_L) and high (RH_H) from Figs. 9–11.

different. This phenomena was consistent with similar observations on GDL tests performed by Ballard Power System Inc. [47].

The MacMullin number as a function of porosity of the seven carbon paper GDLs, Toray TGP-H-060, from this work, are compared with two relevant conductivity models for carbon cloth and carbon paper GDLs, as presented in Martinez et al. [31]. Fig. 8c shows the results, including previous published data [31] of different GDLs. Two separate groups can be observed in this figure. One group corresponds to the carbon cloth GDLs (i.e., materials E, F, and G) which follows the Bruggeman expression ($\varepsilon^{-1.5}$). The second group corresponds to the carbon paper GDLs (i.e., materials A, B, C, and D) which follows the Martinez expression ($\varepsilon^{-3.8}$). However, only the GDLs without MPL from the Toray custom series falls in the group of carbon paper GDLs. The GDLs with MPL from the Toray custom series are grouped with the carbon cloth GDLs.

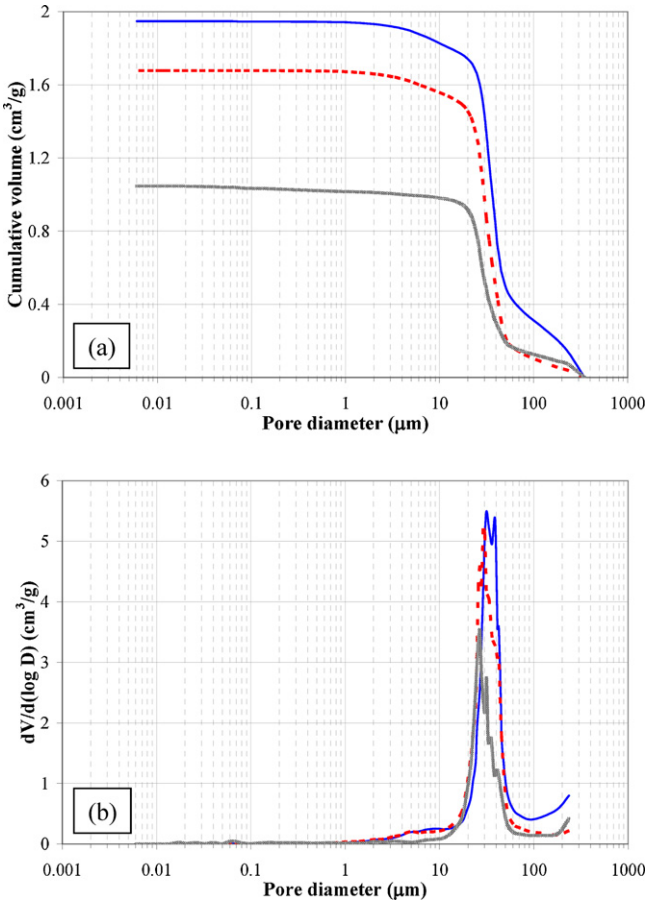

Fig. 5. Porometric curves for (a) integral and (b) differential distribution for Toray TGP-H-060 without MPL. Legend: substrate with no wet proofing (—); substrate with 10% wet proofing (- - -); substrate with 40% wet proofing (▒ ▒ ▒).

The cell performance was obtained at two different humidity conditions, designated as low-end and high-end humidity, using the GDLs of Table 1. Note that the humidity designation is just for convenience in order to differentiate that one humidity is higher than the other. The actual humidity for the condition designated as low-end is 80% and 50% for the anode and cathode, respectively, while the condition designated as high-end is considered under or close to flooding. It is under these conditions that the properties of the MPL become more evident because liquid water has to be removed while other pores need to remain clear to let oxygen reach the catalyst sites. The cell performance obtained in this work was reproduced in order to verify the accuracy of the

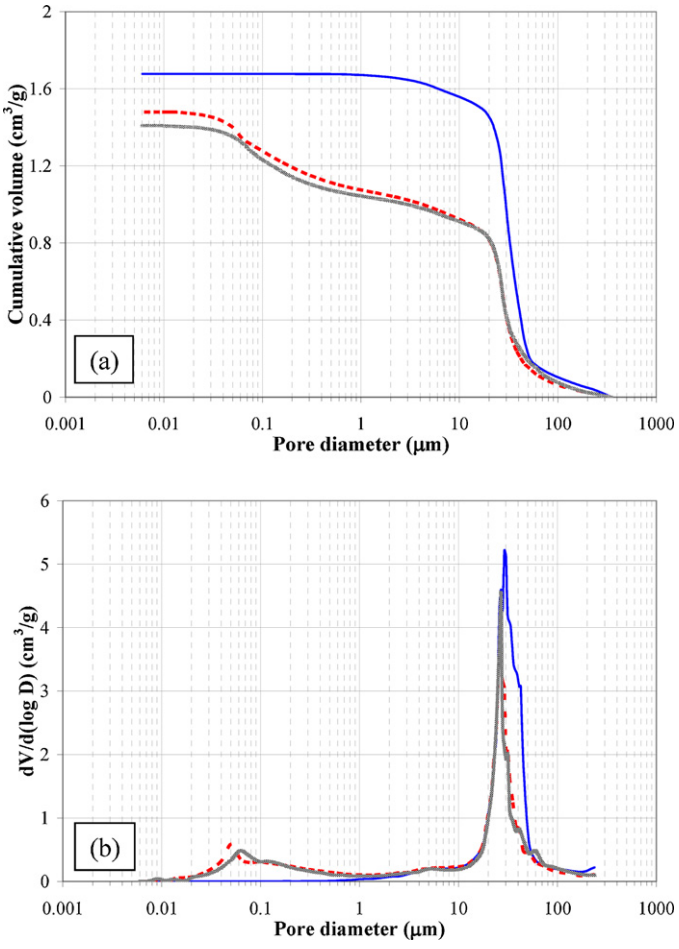

Fig. 6. Porometric curves for (a) integral and (b) differential distribution for Toray TGP-H-060 with 10% wet proofing in the substrate. Legend: substrate only (—); substrate + MPL with 10% wet proofing (- - -); substrate + MPL with 40% wet proofing (▒ ▒ ▒).

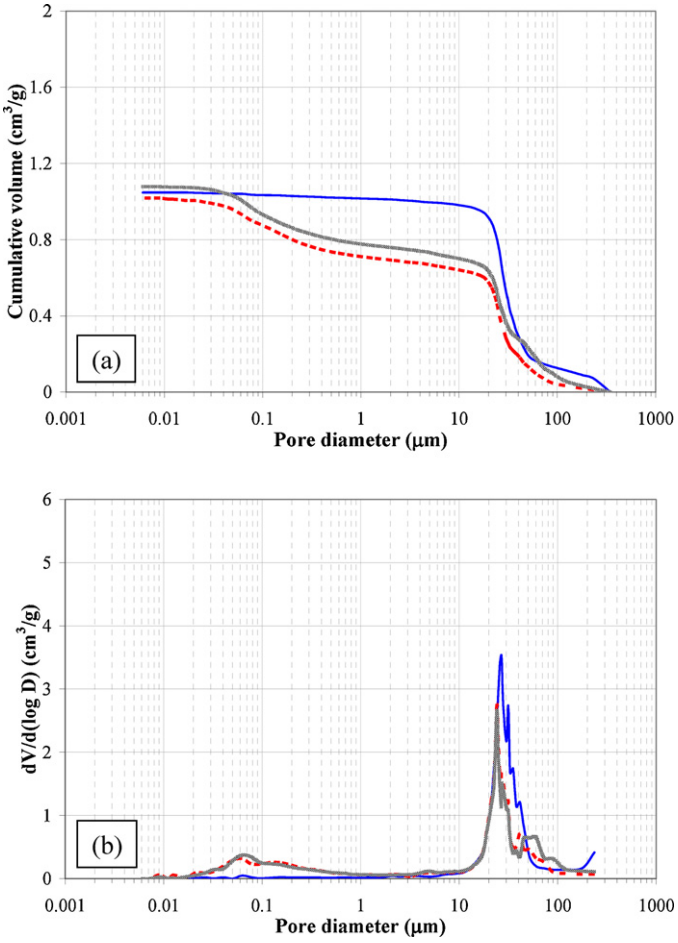

Fig. 7. Porometric curves for (a) integral and (b) differential distribution for Toray TGP-H-060 with 40% wet proofing in the substrate. Legend: substrate only (—); substrate + MPL with 10% wet proofing (- - -); substrate + MPL with 40% wet proofing (▒ ▒ ▒).

measurements. In addition, the ohmic losses for the tested cells were not significant (<80 mV). However, for clarity purposes, the cell performance was corrected for the ohmic losses. Accordingly, the changes in IR-corrected performance, shown in Figs. 9–11, are interpreted in relation to the GDL properties measured in this work and under the conditions tested, but also by incorporating findings from the literature. Note that the cells for the GDL without MPL have comparable performance to those reported in the literature [43,48] under similar conditions. However, some cells show poor performance due to modifications in the structure of the GDL, operating conditions or combination of both. Nevertheless, the objective of this work is to understand the effect of the GDL properties in the MacMullin number and how the latter relates to cell performance.

Table 2 summarizes the GDL property changes due to wet proofing or the addition of the MPL and the respective effects in cell performance. In general, it is difficult to isolate the effect of each parameter because the changes in one parameter will influence others. For example, when the pore volume (porosity) decreases in the GDL it is expected that the cell performance decreases as well because less oxygen is reaching the catalyst. However, under conditions where liquid water is present, the wet proofing treatment (hydrophobicity) is expected to increase performance by providing liquid-water-free paths for gas transport but at the same time it will reduce the porosity of the GDL, which decrease performance. It will also change the tortuosity of the GDL. Consequently, the final effect will depend on the magnitude of each parameter change and whether liquid water is present or not in the GDL. Some of these

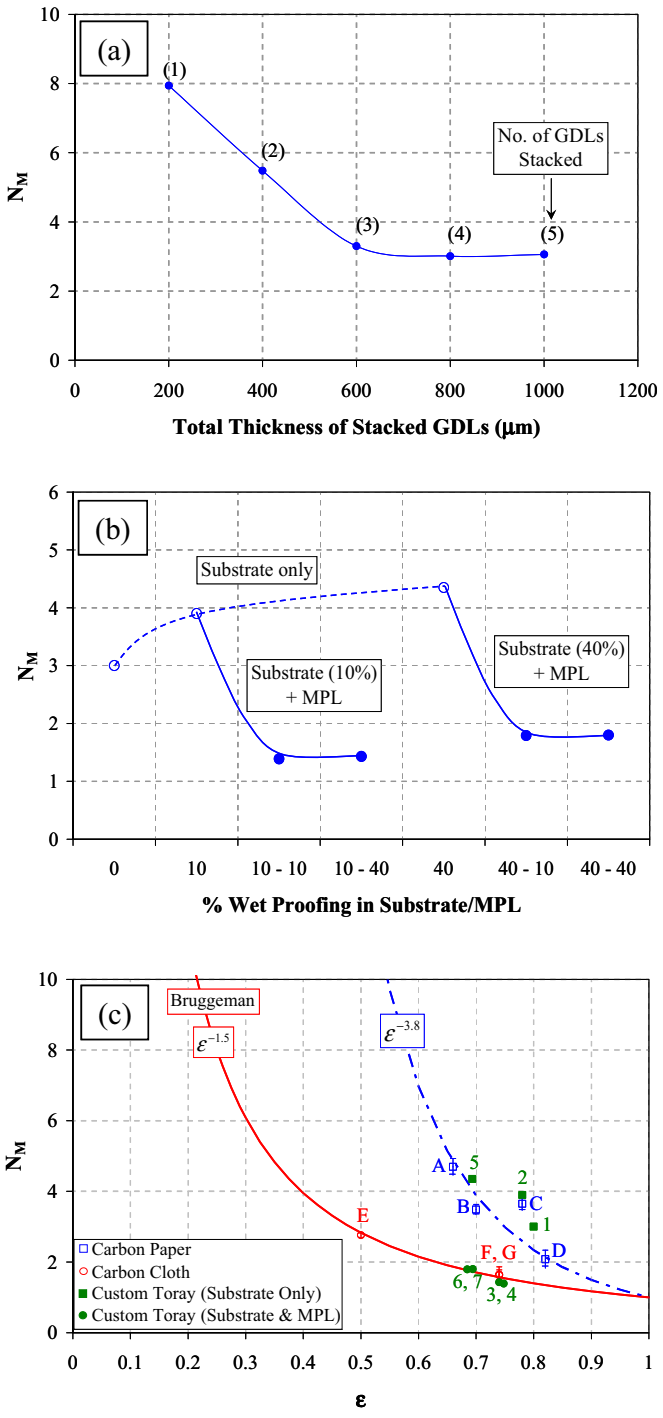

Fig. 8. MacMullin number as function of (a) total thickness of GDLs stacked using GDL 1, (b) wet proofing in substrate and MPL, and (c) porosity. Numbers labels are identified in Table 1. Letters labels correspond to data from Martinez et al. [31] (A) Mitsubishi Rayon PYROFIL MFG-070, (B) Ballard AvCarb P50, (C) Toray TGP-H-120, (D) SGL Carbon SIGRACET 10BB w/MPL, (E) Showa Denko K. K. SCT-NF2-1, (F) W. L. Gore CARBEL CL w/MPL, and (G) E-TEK ELAT LT-1400W w/MPL.

effects are captured in the MacMullin number, which can help to predict the trends in cell performance, but other properties should be considered as well in order to interpret the data.

The thermal conductivity and the water vapor diffusion coefficient have been identified as key properties regarding condensation and water transport in the GDL and/or MPL [35,42,49]. Depending on the formulation used by the authors, these properties appear as a combined quantity which include the bulk and/or effective

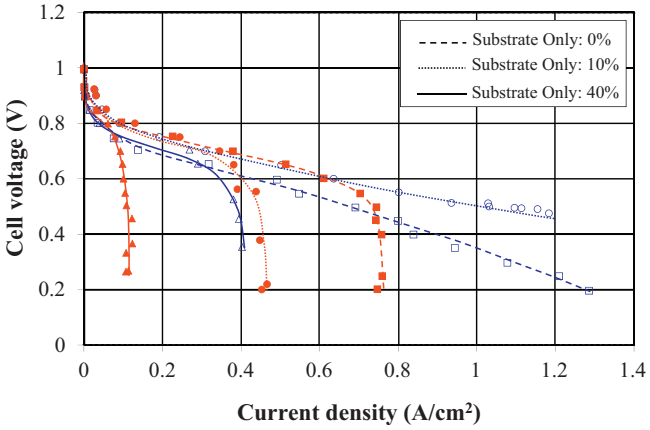

Fig. 9. IR-corrected polarization curves using Toray TGP-H-060 with 0%, 10%, and 40% wet proofing in the substrate at high and low humidification temperatures. Cell temperature is 70 °C and pressure is 101 kPa. Legend: low humidity corresponds to anode/cathode temperatures of 65/55 °C (◯, □, △). High humidity corresponds to anode cathode temperatures of 85/75 °C (●, ■, ▲). Lines have been draw through the data to guide the eyes.

properties. The effective diffusion coefficient is related to the bulk diffusion coefficient through the MacMullin number. Consequently, the lumped quantity can be expressed as κN_M (Table 2). Although details of the effect of thermal conductivity are beyond the scope of this work some particulars have been considered as part of the discussion due to their importance in determining condensation in the GDL.

The thermal conductivity (κ) is also affected by changes in other properties. It decreases with increase in polytetrafluorethylene (PTFE) content [50–52] and porosity [53]. Again, PTFE content decreases the GDL porosity thus the resulting κ will depend on the magnitude change of the two parameters causing an opposite effect in κ. Conversely, it increases with residual water in the GDL [52] and increase in the compressive load [50,54]. An increase in κ can be associated with higher heat transfer in the GDL and better heat dissipation. For the case of N_M, higher values are associated with more flow resistance due to increase in the tortuos path and decrease in porosity. Both of these conditions favor condensation in the GDL. Consequently, an increase in κN_M is generally associated with wetter GDLs [35].

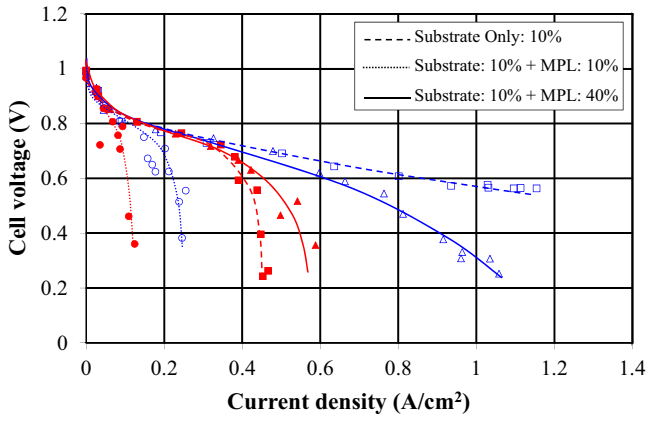

Fig. 10. IR-corrected polarization curves using Toray TGP-H-060 with 10% wet proofing in the substrate at high and low humidification temperatures. Cell temperature is 70 °C and pressure is 101 kPa. Legend: low humidity corresponds to anode/cathode temperatures of 65/55 °C (◯, □, △). High humidity corresponds to anode/cathode temperatures of 85/75 °C (●, ■, ▲). Lines have been draw through the data to guide the eyes.

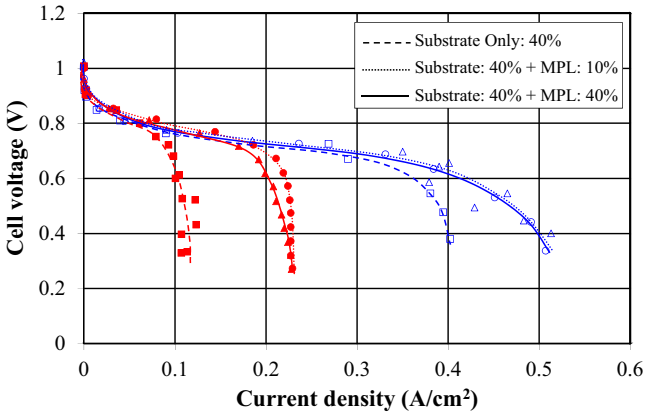

Fig. 11. IR-corrected polarization curves using Toray TGP-H-060 with 40% wet proofing in the substrate at high and low humidification temperatures. Cell temperature is 70 °C and pressure is 101 kPa. Legend: low humidity corresponds to anode/cathode temperatures of 65/55 °C (◯, □, △). High humidity corresponds to anode/cathode temperatures of 85/75 °C (●, ■, ▲). Lines have been draw through the data to guide the eyes.

Fig. 9 compares the IR-corrected cell performance for the GDLs without the MPL. At the high-end humidity (flooding) condition the cell performance decreases as the wet proofing increases. These results cannot be interpreted in terms of κ or κN_M because the resulting change in thermal conductivity cannot be determined. However, the MacMullin number increases with wet proofing, mainly because of the decrease in pore volume as shown in Fig. 5, which is the probable cause for the performance reduction. In other words, the GDL is too wet and the effect of decrease in pore volume predominates over any benefit of the wet proofing. For the low-end humidity condition case the best performance occurs when the GDL with 10% wet proofing is used. In this case, the cell is dryer than the first case and the wet proofing could be helping to maintain the pores free of liquid water. Nevertheless, increasing more the wet proofing caused a performance loss which could be related to a major effect in the decrease of pore volume. As reported in the literature, an optimized PTFE content results due to the trade-off between the pore volume available for the liquid water flow and the water wetting due to the reduced hydrophobic pores [55].

IR-corrected cell performance comparisons for the GDLs with and without the MPL are shown in Figs. 10 and 11 when the wet proofing in the substrate is 10% and 40% respectively. For the GDLs with 10% wet proofing in the substrate (namely GDLs S10 for simplicity) the addition of the MPL with 10% wet proofing decreased the cell performance for both humidity conditions when compared with the base GDL with no MPL. However, for the GDLs with 40% wet proofing in the substrate (GDLs S40) the addition of the MPL increased the cell performance for both humidity conditions when compared with the base GDL (40% wet proofing) with no MPL. Also, the increase of wet proofing in the MPL (from 10% to 40%) improves the performance for the GDLs S10 but does not show a considerably effect in the performance for the GDLs S40. These effects are discussed in details below.

When the MPL is added to the GDLs two opposite effects occurs: (1) a decrease in the pore volume of the substrate region (Figs. 6b and 7b) which is a negative effect and (2) a decrease in the MacMullin number (Fig. 8b) which is a positive effect. In addition, Table 2 shows that the lumped parameter κN_M is expected to decrease for both cases. As discussed above an increase in κN_M is generally associated with wetter GDLs, therefore the decrease in κN_M should result in a dryer GDL. Consequently, the effect of adding the MPL should has resulted in a dryer GDL and better performance. However, this is only observed for the GDLs S40. In terms of porosity, the decrease in pore volume due to the addition of the MPL is

significant for the GDLs S10 as compare to the GDLs S40. Note also that the porosity shown in Table 1 decrease more for the first case than for the second case. Consequently, it is believed that the addition of the MPL to the GDLs S10 decreases the performance due to pore volume reduction.

For the GDLs S10 and S40, when the wet proofing is increased in the MPL there are no significant changes in the overall porosity or the MacMullin number. Although, GDLs S40 do not show improvement in performance, the cells with GDLs S10 show an increase in performance. Table 2 shows that κN_M is expected to decrease for both cases, which should result in dryer GDLs, but only the GDLs S10 show improvement in performance. This may suggest that the considerably higher amount of pore volume in the substrate region (Fig. 5a) for the GDLs S10 results in more volume availability for mass transport than the GDLs S40. Consequently, the benefit of increasing the wet proofing can be observed in the GDLs S10.

The addition of the MPL to the substrate has been associated with improvement in performance. However, it is not always the case. Depending of its properties and the cell operating conditions it can be a detrimental effect. Also, the MPL is not only another layer in the GDL but it also affects the properties of the substrate. Some of the cases can be explained better based on changes in the pore volume available in the substrate for mass transport than using the MacMullin number alone or the lumped factor κN_M.

The MacMullin number measurements can help to understand critical properties of gas diffusion media that impact directly the liquid water and gas transport in fuel cells. It includes assessing the length (derived from the MacMullin number) through which these phases travel. Previously, only measurements of the porosity were used to characterize the GDL and still product data sheets only use porosity. Mathematical models for fuel cell can also be improved by the use of the actual path length which leads to accurate calculations on liquid and gas transport through the GDL. The use of this technique can provide the industry the knowledge to improve the design of GDL and reduce their cost by leading it to consider the path length for liquid and gas transport as part of their research.

4. Conclusions

In this work, a detailed structure characterization of a custom series of Toray carbon paper GDLs was performed by measuring the MacMullin number, the PSD, through analysis of SEM images, and tested under low and high humidity conditions in a fuel cell. SEM images correlated very well with the data shown for PSD. Distinction between the substrate layer and the MPL were clearly shown as two different slopes in the integral distribution and two different peaks in the differential distribution. The effect of the MPL and wet proofing in the MacMullin number has been evaluated. The MacMullin number increased with increase in wet proofing but decreased with the addition of the MPL. Additional results showed that the addition of the MPL can affect the cell performance negatively or positively. However, the changes cannot be explained by using the MacMullin number alone or the lumped factor κN_M but by considering the combined effect of the substrate and MPL properties as well as the cell operating conditions. Therefore, the effect of the MPL may depend on the operating conditions and the GDL design.

The observations presented in this work highlight the importance of several parameters that need to be taken into account to evaluate the behavior in the cell performance. The results suggest that the available pore volume (porosity) and the path length (tortuosity) are integral part of the complex interaction that exits between the MPL and the substrate. Both, wet proofing and the addition of the MPL, affect the pore volume and change the path length for liquid and gas transport. However, these changes occur simultaneously and are difficult to decouple. Although thermal conductivity has been identified in the literature as a key parameter as well, it is also affected by the wet proofing and the MPL addition. Consequently, the MacMullin number is a key parameter that should be included as part of the GDL characterization and product data sheets. It contains the missing information for the path length in GDLs, which is generally approximated with the Bruggeman expression. It is an important property that can improve fuel cell mathematical models and leads to better GDL designs.

Acknowledgments

This research was supported by the National Science Foundation of Industrial/University Collaborative Research Center for Fuel Cells (EEC-0324260). This work was also partially supported by the Department of Energy (DE-EE0000471).

References

[1] L. Cindrella, A.M. Kannan, J.F. Lin, K. Saminathan, Y. Ho, C.W. Lin, J. Wertz, Journal of Power Sources 194 (2009) 146–160.
[2] Z.G. Qi, A. Kaufman, Journal of Power Sources 109 (2002) 38–46.
[3] A.Z. Weber, J. Newman, Journal of the Electrochemical Society 152 (2005) A677.
[4] H. Atiyeh, K. Karan, B. Peppley, A. Phoenix, E. Halliop, J. Pharoah, Journal of Power Sources 170 (2007) 111–121.
[5] T. Kim, S. Lee, H. Park, International Journal of Hydrogen Energy 35 (2010) 8631–8643.
[6] J.H. Chun, K.T. Park, D.H. Jo, J.Y. Lee, S.G. Kim, S.H. Park, E.S. Lee, J.Y. Jyoung, S.H. Kim, International Journal of Hydrogen Energy 36 (2011) 8422–8428.
[7] J. Chen, H. Xu, H. Zhang, B. Yi, Journal of Power Sources 182 (2008) 531–539.
[8] W.-M. Yan, D.-K. Wu, X.-D. Wang, A.-L. Ong, D.-J. Lee, A. Su, Journal of Power Sources 195 (2010) 5731–5734.
[9] X.L. Wang, H.M. Zhang, J.L. Zhang, H.F. Xu, X.B. Zhu, J. Chen, B.L. Yi, Journal of Power Sources 162 (2006) 474–479.
[10] S. Park, J. Lee, B. Popov, Journal of Power Sources 163 (2006) 357–363.
[11] A. Su, C.Y. Hsu, F.B. Weng, P. Mu, W. Shenlong, H. Zhoufa, Proceedings of the Institution of Mechanical Engineers A: Journal of Power and Energy 224 (2010) 179–184.
[12] J.H. Chun, K.T. Park, D.H. Jo, J.Y. Lee, S.G. Kim, E.S. Lee, J.-Y. Jyoung, S.H. Kim, International Journal of Hydrogen Energy 35 (2010) 11148–11153.
[13] C.-J. Tseng, S.-K. Lo, Energy Conversion and Management 51 (2010) 677–684.
[14] G. Velayutham, J. Kaushik, N. Rajalakshmi, K.S. Dhathathreyan, Fuel Cells 7 (2007) 314–318.
[15] S. Park, J.-W. Lee, B.N. Popov, Journal of Power Sources 177 (2008) 457–463.
[16] M. Ahn, Y.-H. Cho, Y.-H. Cho, J. Kim, N. Jung, Y.-E. Sung, Electrochimica Acta 56 (2011) 2450–2457.
[17] R. Schweiss, M. Steeb, P.M. Wilde, Fuel Cells 10 (2010) 1176–1180.
[18] M.S. Ismail, D. Borman, T. Damjanovic, D.B. Ingham, M. Pourkashanian, International Journal of Hydrogen Energy 36 (2011) 10392–10402.
[19] J.T. Gostick, M.A. Ioannidis, M.W. Fowler, M.D. Pritzker, Electrochemistry Communications 11 (2009) 576–579.
[20] Z.J. Lu, M.M. Daino, C. Rath, S.G. Kandlikar, International Journal of Hydrogen Energy 35 (2010) 4222–4233.
[21] K. Kang, H. Ju, Journal of Power Sources 194 (2009) 763–773.
[22] J.H. Nam, K.-J. Lee, G.-S. Hwang, C.-J. Kim, M. Kaviany, International Journal of Heat and Mass Transfer 52 (2009) 2779–2791.
[23] F.E. Hizir, S.O. Ural, E.C. Kumbur, M.M. Mench, Journal of Power Sources 195 (2010) 3463–3471.
[24] X. Wang, T. Van Nguyen, Journal of the Electrochemical Society 157 (2010) B496.
[25] R. Wu, X. Zhu, Q. Liao, H. Wang, Y.-d. Ding, J. Li, D.-d. Ye, International Journal of Hydrogen Energy 35 (2010) 7588–7593.
[26] R. Wu, X. Zhu, Q. Liao, H. Wang, Y.-d. Ding, J. Li, D.-d. Ye, International Journal of Hydrogen Energy 35 (2010) 9134–9143.
[27] A.Z. Weber, Journal of Power Sources 195 (2010) 5292–5304.
[28] J.T. Gostick, M.A. Ioannidis, M.D. Pritzker, M.W. Fowler, Journal of the Electrochemical Society 157 (2010) B563–B571.
[29] E. Nishiyama, T. Murahashi, Journal of Power Sources 196 (2011) 1847–1854.
[30] J.S. Preston, R.S. Fu, U. Pasaogullari, D.S. Hussey, D.L. Jacobson, Journal of the Electrochemical Society 158 (2011) B239.
[31] M.J. Martínez, S. Shimpalee, J.W. Van Zee, Journal of the Electrochemical Society 156 (2009) B80–B85.
[32] J. Bear, Dynamics of Fluids in Porous Media, Dover Publications, Inc., New York, 1972.
[33] D.R. Baker, C. Wieser, K.C. Neyerlin, M.W. Murphy, ECS Transactions 3 (2006) 989–999.
[34] D.R. Baker, D.A. Caulk, K.C. Neyerlin, M.W. Murphy, Journal of the Electrochemical Society 156 (2009) B991–B1003.
[35] D.A. Caulk, D.R. Baker, Journal of the Electrochemical Society 157 (2010) B1237–B1244.

[36] D. Kramer, S.A. Freunberger, R. Fluckiger, I.A. Schneider, A. Wokaun, F.N. Buchi, G.G. Scherer, Journal of Electroanalytical Chemistry 612 (2008) 63–77.
[37] R. Fluckiger, S.A. Freunberger, D. Kramer, A. Wokaun, G.G. Scherer, F.N. Buchi, Electrochimica Acta 54 (2008) 551–559.
[38] M.J. Martínez, S. Shimpalee, J.W. Van Zee, Journal of the Electrochemical Society 156 (2009) B558–B564.
[39] T. Kitahara, T. Konomi, H. Nakajima, Journal of Power Sources 195 (2010) 2202–2211.
[40] T. Kitahara, T. Konomi, H. Nakajima, M. Kazama, Journal of Environment and Engineering 6 (2011) 17–27.
[41] Z. Fishman, A. Bazylak, Journal of the Electrochemical Society 158 (2011) B846–B851.
[42] J.P. Owejan, J.E. Owejan, W.B. Gu, T.A. Trabold, T.W. Tighe, M.F. Mathias, Journal of the Electrochemical Society 157 (2010) B1456–B1464.
[43] G.G. Park, Y.J. Sohn, T.H. Yang, Y.G. Yoon, W.Y. Lee, C.S. Kim, Journal of Power Sources 131 (2004) 182–187.
[44] G.Y. Lin, T. Van Nguyen, Journal of the Electrochemical Society 152 (2005) A1942–A1948.
[45] Z. Fishman, A. Bazylak, Journal of the Electrochemical Society 158 (2011) B841–B845.
[46] J.T. Gostick, M.W. Fowler, M.A. Ioannidis, M.D. Pritzker, Y.M. Volfkovich, A. Sakars, Journal of Power Sources 156 (2006) 375–387.
[47] Ballard Material Products Division, Ballard Power System Inc., 2010.
[48] R.P. Ramasamy, E.C. Kumbur, M.M. Mench, W. Liu, D. Moore, M. Murthy, International Journal of Hydrogen Energy 33 (2008) 3351–3367.
[49] S.F. Burlatsky, V.V. Atrazhev, M. Gummalla, D.A. Condit, F.Q. Liu, Journal of Power Sources 190 (2009) 485–492.
[50] G. Karimi, X. Li, P. Teertstra, Electrochimica Acta 55 (2010) 1619–1625.
[51] N. Zamel, E. Litovsky, S. Shakhshir, X.G. Li, J. Kleiman, Applied Energy 88 (2011) 3042–3050.
[52] O.S. Burheim, J.G. Pharoah, H. Lampert, P.J.S. Vie, S. Kjelstrup, Journal of Fuel Cell Science and Technology 8 (2011).
[53] N. Zamel, X.G. Li, J. Shen, J. Becker, A. Wiegmann, Chemical Engineering Science 65 (2010) 3994–4006.
[54] E. Sadeghi, N. Djilali, M. Bahrami, Journal of Power Sources 196 (2011) 246–254.
[55] S. Park, B.N. Popov, Fuel 88 (2009) 2068–2073.